Experimental Mechanics (2020) 60:165–170
https://doi.org/10.1007/s11340-019-00558-4

BRIEF TECHNICAL NOTE

Tracking Defects and Microstructural Heterogeneities in Meso-Scale Tensile Specimens Excised from Additively Manufactured Parts

J.T. Benzing[1] · L.A. Liew[1] · N. Hrabe[1] · F.W. DelRio[1]

Received: 23 July 2019 / Accepted: 9 October 2019 / Published online: 24 October 2019

Abstract

The commercialization of additive manufacturing (AM) is underway in the aerospace and biomedical device industries [1, 2]. However, most metal parts produced by AM are limited to non-critical applications, since the various processes produce internal porosity, anisotropy, and microstructural heterogeneities [1, 3]. It has been implied that small-scale mechanical tests can advance measurement standards for AM applications by probing the effects of defects and heterogeneities on mechanical properties at more appropriate length scales [4, 5]. Traditionally, small-scale techniques have been used to characterize location- and orientation-specific mechanical properties in wrought materials [6–10]. A common method for excising mechanical test specimens from bulk parts with negligible influence on specimen integrity involves electrical discharge machining (EDM) [11]. This work demonstrates that excising meso-scale tensile specimens from additively manufactured parts enables tracking of subsurface and visible features of interest (porosity and microstructural heterogeneities) throughout the entire gauge section such that the individual contributions to deformation behavior can be assessed.

Keywords Additive manufacturing (AM) · Ti-6Al-4V · Meso-scale · Tension test · Electron backscatter diffraction (EBSD) · X-ray computed tomography (CT)

Experimental Methods

Ti-6Al-4V parts (35 mm tall, 25 mm wide, and 15 mm thick) were fabricated by electron-beam melting powder-bed fusion (EBM-PBF) using an Arcam[1] A1 machine (software version 3.2.132, 60 kV accelerating voltage, 50 μm layer thickness, speed factor 35) and Arcam Ti-6Al-4V gas-atomized powder (average diameter approximately 70 μm).

Two wafers (2 mm thickness) were sliced off the Ti-6Al-4V part with a high-speed saw. One wafer was ground to 0.8 mm and the other to 0.25 mm (final griding step used 800 grit SiC paper). Meso-scale tensile specimens (0.5 mm gauge width and 2 mm gauge length) were excised from each wafer by wire EDM (through a commercial vendor), such that the tensile direction was perpendicular to the build direction. The 0.8 mm thick meso-scale specimens were thinned to an approximate thickness of 0.19 mm using standard polishing procedures (SiC paper, 1 μm diamond particle suspension, and 50 nm colloidal silica). To measure bulk properties, ten larger tensile specimens (gauge dimensions: 2.5 mm width, 5 mm length, and 1.3 mm thickness) were excised from the Ti-6Al-4V part using EDM.

Microstructural characterization and fractography were performed using an optical microscope and a field-emission scanning electron microscope (FE-SEM) operated at 20 kV for electron backscatter diffraction (EBSD) measurements, backscattered electron imaging, and secondary electron imaging. The FE-SEM was operated at 6 kV for energy dispersive spectroscopy (EDS) measurements. Specimens were analyzed for internal porosity with X-ray computed tomography (CT) at 80 kV with a 1.8 μm voxel size.

[1] Certain commercial software, equipment, instruments or materials are identified in this paper to adequately specify the experimental procedure. Such identification is not intended to imply recommendation or endorsement by the National Institute of Standards and Technology, nor is it intended to imply that the equipment or materials identified are necessarily the best available for the purpose.

✉ J. T. Benzing
jake.benzing@nist.gov

[1] Applied Chemicals and Materials Division, National Institute of Standards and Technology, 325 Broadway, MS-647 Boulder CO 80305 USA

Two meso-scale tensile specimens were deformed at a strain rate of 1×10^{-3} s^{-1} in uniaxial tension, and an optical microscope was used to measure strain via digital image correlation. One specimen underwent a tension test. The second specimen was pulled past yielding, removed from the testing apparatus and microstructural characterization performed, and then was re-mounted in the testing apparatus and pulled to failure. The specimen design, test apparatus, and test and analyses methods were previously described [12]. ASTM E8 was used as a basis for the specimen geometry, but with adaptations to accommodate the smaller size. For example, pin-loading was used which is consistent with E8, and E8 specifies a width to thickness ratio of at least 0.78, which is met by the current geometry, but a major deviation from ASTM E8 is the width to length ratio used in this work because the gauge length was shortened from a previous design [12] due to the amount of material available. Gauge dimensions were determined by optical microscopy and corroborated by X-ray CT. The thickness of polished meso-scale specimen ranged from 183 μm to 191 μm. The measurement uncertainty was 2% and the standard deviation in thickness for each meso-scale specimen was approximately 3 μm.

Results

The side walls along the gauge length of each meso-scale tensile specimen were straight (Fig. 1a). The re-cast layer (produced by EDM) only existed on surfaces of the side walls (Fig 1 a_1), except for some instances of spatter onto the top surface (Fig. 1$a_{2\text{-}3}$), which was easily removed with mechanical polishing and did not change other gauge dimensions (Fig. 1b). The re-cast layer thickness was estimated to be less than 5 μm (Fig 1a_4) and is considered thin when compared to the gauge width (500 μm). A cross-sectional view of the gauge section in the polished meso-scale specimen indicates the only effect from mechanical polishing of meso-scale specimens was minor rounding near the edges of the top surface (arrows in Fig 1b_1).

To provide a more quantitative analysis of the re-cast layer and other effects from EDM, an undeformed meso-scale specimen was mounted in conductive Bakelite and polished down to the mid thickness (Fig 1$b_{2\text{-}5}$). The re-cast layer consisted of amorphous material and a V-rich oxide (Fig 1b_5) that ranged in thickness between 1 μm and 5 μm (Fig 1b_2). The heat-affected zone (HAZ) resembled the base microstructure in terms of chemistry (Fig. 1b_5), grain morphology (Fig. 1$b_{4\text{-}5}$) and grain orientation (Fig. **1**b_4). However, the HAZ contained a higher dislocation content (Fig. 1b_5), which is quantitatively represented by the degradation in image quality (Fig. 1b_3), *i.e.* a metric with a linear scale that is used to describe the sharpness of diffraction patterns. The HAZ thickness ranges between 3 μm and 7 μm (Fig. 1 $b_{2\text{-}3}$). Given the extremes of each, the combined thickness of the re-cast layer and heat-affected zone constitutes 1.6% to 4.8% of the gauge width.

A survey with optical microscopy identified areas of interest on surfaces of polished (not mounted) meso-scale tensile specimens before, during, and after deformation (Fig. 2). Before tensile deformation (Fig. 2a_1), the optical image simply highlighted locations of pores exposed to the surface. X-ray CT provided a quantitative description of the size and location of each individual pore throughout the entire volume of the gauge section (tracked before and after deformation). Since tensile specimens were excised from the as-built condition, spherical gas pores were observed, but no gross lack-of-fusion was found in the gauge section (Fig. 2a_2). Porosity comprised 0.12% of the volume in the gauge section, and most pores were less than 12 μm in diameter.

The as-built microstructure of EBM-PBF Ti-6Al-4V was primarily composed of α laths and β remnants. Based on EBSD unique grain maps, the α lath thickness in the as-built condition was 1.19 μm ± 0.24 μm. EBSD maps of grain orientation and Schmid factor (Fig. 2 $a_{3\text{-}4}$) show grain boundary α elongated in the build direction, plus regions in the center and right side of the gauge length where slip was likely to occur first (based on the surface microstructure).

Following interruption of the tension test, optical microscopy revealed surface relief/strain localizations in the center and right side of the gauge section. Figure 2b highlights three categories of defects: microstructural heterogeneities that intersected gas pores exposed to the surface (Fig. 2 $b_{2\text{-}3}$), microstructural heterogeneities that spanned most of the gauge width (Fig. 2 $b_{4\text{-}5}$), and large gas pores (Fig. 2 $b_{6\text{-}7}$). Further examination of these microstructural heterogeneities indicated most strain localizations corresponded to large α grains.

After tensile deformation to failure, characterization of the meso-scale specimen showed that fracture occurred (Fig. 2c_2) along grain boundary α (formed along a prior-β grain boundary) that spanned most of the gauge width (Fig. 2 $b_{\mathbf{1,4}}$). Internal gas pores and pores exposed to the surface also showed signs of strain localization. The surface-exposed pore (dashed pentagon in Fig. 2 a_2**)** and the spherical internal pore (dashed circle in Fig. 2 a_2) both lengthened in the direction of tension. Before deformation, the width (dimension parallel to the tensile direction) of the surface-exposed pore was 51 μm. This dimension increased to 55 μm after interruption and to 59 μm after failure. Similar changes were observed for the internal pore (46 μm, 48 μm, and 55 μm). The internal pore volume increased by 8.8% (before deformation compared to after final fracture).

Figure 3a shows the engineering stress-strain responses for specimens pulled to failure without interruption for both the

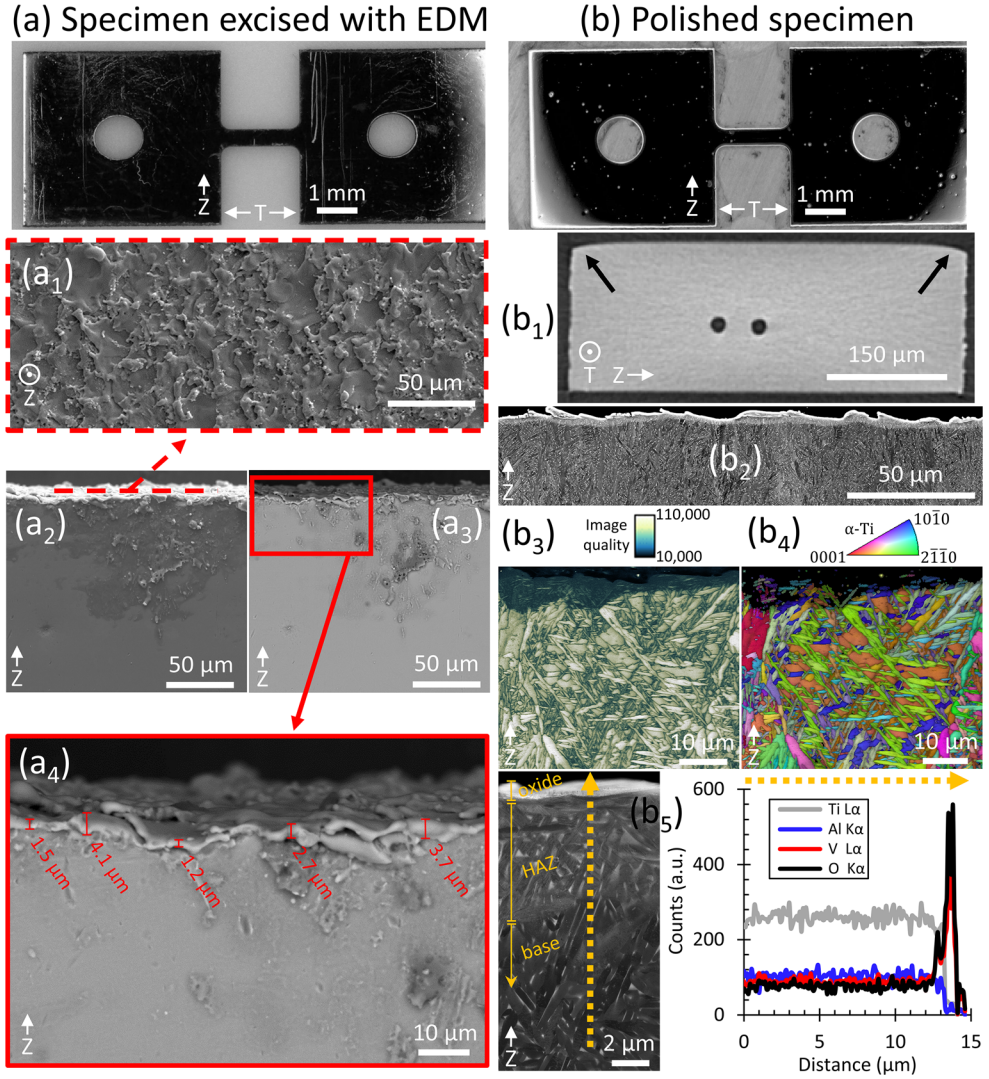

Fig. 1 Optical images of the entire meso-scale tensile specimen (grip to grip length is 2 mm) were recorded (top view) for the following conditions: (**a**) as-received following EDM (gauge cross-section is 0.25 mm thick by 0.5 mm wide) and (**b**) polished (cross-section is 0.19 mm thick by 0.5 mm wide), where Z is the build direction and T is the direction of tension. The EDM process produces (**a**) straight side walls. The ($\mathbf{a_1}$/$\mathbf{a_2}$) secondary electron images and ($\mathbf{a_3}$/$\mathbf{a_4}$/$\mathbf{b_2}$/$\mathbf{b_5}$) backscattered electron images show: the top view of the gauge section in the ($\mathbf{a_2}$/$\mathbf{a_3}$/$\mathbf{a_4}$) as-received and ($\mathbf{b_2}$/$\mathbf{b_5}$) polished conditions. A side view of the ($\mathbf{a_1}$) surface quality of the re-cast layer on the side walls is provided. Polishing produced a ($\mathbf{b_1}$) small amount of rounding near the edges of the top surface and is visible with X-ray CT (see arrows) in a view of the cross-section (note: internal pores, *i.e.* black circles, are also visible). The ($\mathbf{a_4}$) estimated thickness of the re-cast layer ranges from 1 µm to 5 µm and contains a thin layer of V-rich oxide, based on a line-scan using ($\mathbf{b_5}$) energy dispersive spectroscopy. Near the re-cast layer is a heat-affected zone (HAZ), which resembles the base microstructure in terms of ($\mathbf{b_5}$) composition, ($\mathbf{b_4}$/$\mathbf{b_5}$) grain morphology, and ($\mathbf{b_4}$) grain orientation. The HAZ microstructure is somewhat diffuse (compared to the base microstructure) due to a higher dislocation content ($\mathbf{b_5}$) and lower diffraction pattern quality ($\mathbf{b_3}$). The thickness of the HAZ ranges from 3 µm to 7 µm

meso-scale and bulk tensile specimen geometries. For reference, the ultimate tensile strength and total elongation of the bulk properties were 973 MPa and 0.128, respectively. Fractography revealed ductile failure from microvoid coalescence on all fracture surfaces in all meso-scale and bulk tensile specimens. An image of an entire meso-scale fracture surface (Fig. 3b) revealed spherical gas pores (Fig. 3 b_1) and ridges elongated in the build direction (Fig. 3 b_2).

Discussion

The principal benefit of meso-scale mechanical testing and characterization is the specimen size and length scale allows for investigation of which defects and microstructural heterogeneities contained in the gauge section most likely contribute to localized deformation and failure [4]. Also, surface-based microstructure characterization (*e.g.*, EBSD) tends to be

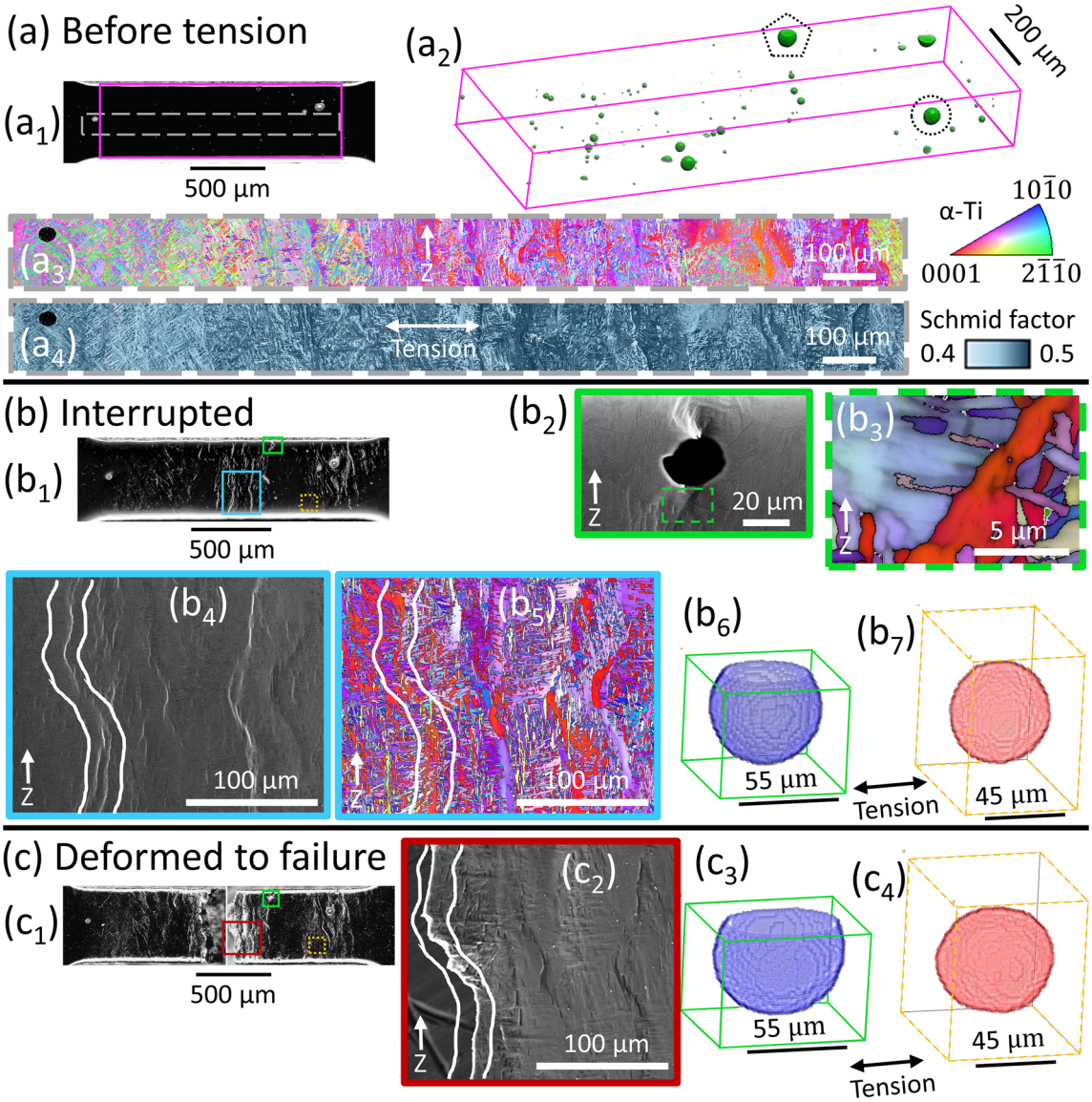

Fig. 2 Optical images of the entire polished meso-scale tensile specimen (top view) were recorded ($\mathbf{a_1}$) before tension, ($\mathbf{b_1}$) after interruption, and ($\mathbf{c_1}$) after deformation to failure. An ($\mathbf{a_2}$) X-ray CT reconstruction of porosity highlights the locations of all pores larger than 3 µm (diameter) throughout the gauge section. The surface-exposed pore identified with a pentagon in ($\mathbf{a_2}$) is the same pore shown in ($\mathbf{b_2}$), ($\mathbf{b_6}$), and ($\mathbf{c_3}$), while the circled sub-surface pore in ($\mathbf{a_2}$) is the pore shown in ($\mathbf{b_7}$) and ($\mathbf{c_4}$). Before tension, ($\mathbf{a_3}$/$\mathbf{a_4}$) EBSD maps spanning the entire gauge length were recorded to understand how ($\mathbf{a_3}$) grain orientation, grain morphology, and ($\mathbf{a_4}$) Schmid factor influence strain localizations. After interruption, the meso-scale specimen was examined with ($\mathbf{b_3}$/$\mathbf{b_5}$) EBSD in areas of visible surface-relief/strain localization. ($\mathbf{c_2}$) Failure occurred along previously identified areas of surface relief (see white lines), plus ($\mathbf{c_3}$/$\mathbf{c_4}$) both types of pores were elongated in the direction of tension

representative of the microstructure through the entire specimen thickness for specimens this small. This facilitates a deeper understanding of the microstructural effects on deformation behavior. While wire EDM is a viable technique for excising macro- and meso-scale specimens from wrought materials [6–10], excising meso-scale tensile specimens from additively manufactured parts enables probing of unique structure-property relationships without influence from as-built surfaces. Wire EDM used in this work produced straight side walls along the gauge length, a thin re-cast layer (less than a few µm) of oxide, and a thin heat-affected zone that still resembled the bulk microstructure in terms of grain morphology, orientation, and chemistry (Fig. 1). Even though dimensions of the gauge cross-section were on the order of a few hundred µm, the tensile properties of the meso-scale specimen still exceeded the minimum ASTM requirements (0.10 engineering strain) for additively manufactured [13] and wrought products [14], although more mesoscale specimens would need to be tested to confirm this definitively. While there is a clear difference in the values of uniform and total elongation,

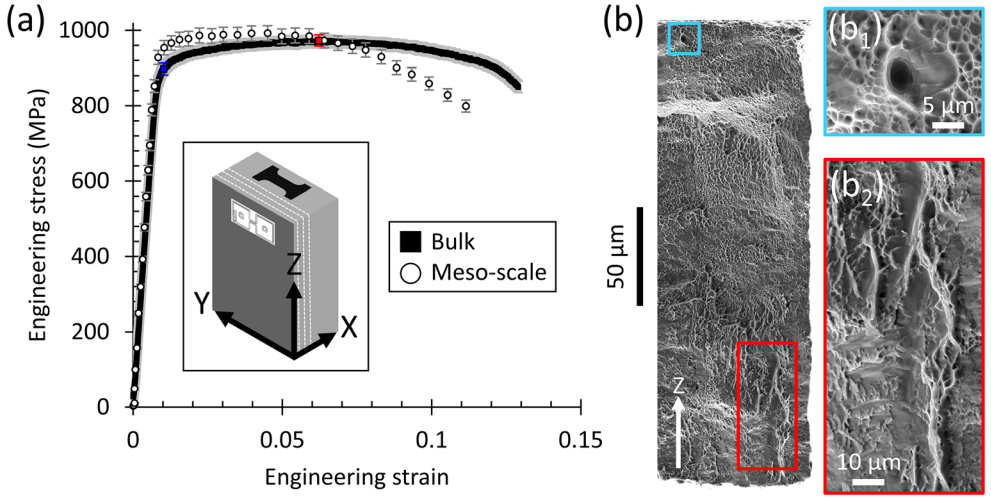

Fig. 3 Tensile properties of a meso-scale sized specimen excised from Ti-6Al-4V parts (produced by EBM-PBF methods) and pulled to failure without interruption is compared with bulk tensile properties of the same EBM-PBF build. (**a**) Representative engineering stress-strain curve of bulk specimens and a meso-scale tensile specimen, where the inset of the Ti-6Al-4V part shows wafer orientations (dashed lines), specimen orientation, and build direction. Error bars on the bulk engineering stress values are based on one standard deviation from 10 tests (yield strength is the blue square and ultimate tensile strength is the red square). Error bars on the meso-scale stress values are based on measurement uncertainty with respect to the initial cross-sectional area of the specimen (excised from the 0.25 mm thick wafer). Secondary electron images were recorded from the (**b**) fracture surface of a meso-scale specimen and highlight the presence of microvoid coalescence, ($\mathbf{b_1}$) gas porosity, and ($\mathbf{b_2}$) elongated features that are parallel to the build direction

the ultimate tensile strengths of the meso-scale and bulk specimens do not differ significantly. However, the yield strengths and initial strain hardening behaviors do differ. The differences in tensile properties are attributed to differences in specimen orientation (different horizontals with respect to build direction), local variations in crystallographic texture, and the number of grain-boundary α (approximately 15) present in the thickness of the meso-scale specimen. The latter assumes there are only grain-boundary α present in the gauge thickness (an extreme scenario), but the microstructure is predominantly made up of thin α laths. The current gauge thickness likely contains on the order of 50 to 150 α laths, depending on the arrangement, and should thus not produce significant scatter, based on the number of grains in the gauge cross-section [15]. Future work will compare a statistically relevant number of meso-scale tensile tests with bulk tensile properties that are all measured with the same specimen orientation (with respect to build direction).

Failure did not occur at a spatially-local maxima of pore density, most likely because the largest spherical gas pore was 51 μm, the porosity content comprised only 0.12% of the gauge volume, and no lack-of-fusion zones were observed (only spherical pores). Ultimately, this means that microstructural heterogeneities contributed the most to localized deformation (Fig. 2). These heterogeneities (grain boundary α elongated in the build direction) have been reported [16] as contributors to anisotropy in mechanical properties, since these grains form along prior-β grain boundaries. Previous work [17, 18] has used meso-scale tensile specimens to study AM metals, but none tracked microstructural heterogeneities during deformation as was accomplished in this work. This tracking is necessary to understand microstructure effects on deformation behavior of these complex materials.

Conclusions

In this work, meso-scale tensile specimens were excised from bulk additively manufactured Ti-6Al-4V parts using wire EDM. To better understand structure-property relationships in additively manufactured parts, EBSD and X-ray CT measurements were completed before and after quasi-static tension tests (including an interruption after yielding) to track the evolution of microstructural heterogeneities and changes in porosity throughout the entire gauge length of the tensile specimen. While internal and surface-exposed pores did elongate in the tensile direction, failure ultimately occurred near a microstructural heterogeneity (grain boundary α elongated in the build direction).

Acknowledgements This research was performed while Jake Benzing held a National Research Council Postdoctoral Research Associateship at the National Institute of Standards and Technology.

References

1. Hrabe N, Barbosa N, Daniewicz SR, Shamsaei N (2016) Findings from the NIST/ASTM Workshop on Mechanical Behavior of Additive Manufacturing Components. NIST Adv Manuf Ser:1–256. https://doi.org/10.6028/NIST.AMS.100-4
2. Conner BP, Manogharan GP, Martof AN, Rodomsky LM, Rodomsky CM, Jordan DC, Limperos JW (2014) Making sense of 3-D printing: Creating a map of additive manufacturing products

and services. Addit Manuf 1:64–76. https://doi.org/10.1016/j.addma.2014.08.005
3. Seifi M, Gorelik M, Waller J, Hrabe N, Shamsaei N, Daniewicz S, Lewandowski JJ (2017) Progress Towards Metal Additive Manufacturing Standardization to Support Qualification and Certification. Jom. 69:439–455. https://doi.org/10.1007/s11837-017-2265-2
4. Gorelik M (2017) Additive manufacturing in the context of structural integrity. Int J Fatigue 94:168–177. https://doi.org/10.1016/j.ijfatigue.2016.07.005
5. M.P. Gallaher, Z.T. Oliver, K.T. Reith, A.C. O'Connor (2016) Economic Analysis of Technology Infrastructure Needs for Advanced Manufacturing: Smart Manufacturing. doi:https://doi.org/10.6028/NIST.GCR.16-007
6. Poling WA (2012) Grain size effects in micro-tensile testing of austenitic stainless steel, Master's thesis, Department of Metallurgical and Materials Engineering, Colorado School of Mines
7. Nimer S, Wolk J, Zupan M (2013) Local property characterization of friction stir welded Ti-5111: Transverse orientation measurements. Acta Mater 61:3050–3059. https://doi.org/10.1016/j.actamat.2013.01.065
8. Dehm G, Jaya BN, Raghavan R, Kirchlechner C (2018) Overview on micro- and nanomechanical testing: New insights in interface plasticity and fracture at small length scales. Acta Mater 142:248–282. https://doi.org/10.1016/j.actamat.2017.06.019
9. Savage MF, Tatalovich J, Zupan M, Hemker KJ, Mills MJ (2001) Deformation mechanisms and microtensile behavior of single colony Ti-6242Si. Mater Sci Eng A 319–321:398–403. https://doi.org/10.1016/S0921-5093(01)01024-3
10. Benzing JT, He M, Vivek A, Taber GA, Mills MJ, Daehn GS (2017) A Microsample Tensile Test Application: Local Strength of Impact Welds Between Sheet Metals. J Mater Eng Perform 26:1229–1235. https://doi.org/10.1007/s11665-017-2514-0
11. Singh SK, Mali HS (2019) Microfeatures and microfabrication: Current role of micro-electric discharge machining. J Micromechanics Microengineering 29:043002. https://doi.org/10.1088/1361-6439/ab0249
12. Liew LA, Read DT, White RM, Barbosa N (2018) U.S. Army ARDEC Joint Fuze Technology Program (JFTP) Task 2 report: quasi-static tensile tests of microfabricated electrodeposited (LIGA) Ni alloys. NIST Interagency/Internal Report 8182. doi: https://doi.org/10.6028/NIST.IR.8182
13. ASTM International (F3001), ASTM F3001 - Standard Specification for Additive Manufacturng Titanium-6 Aluminum-4 Vanadium ELI (Extra Low Interstitial) with Powder Bed Fusion, in: West Conshohocken, PA, 2014. doi:https://doi.org/10.1520/F3001-14
14. ASTM International (F1472), ASTM F1472 - Standard Specification for Wrought Titanium-6Aluminum-4Vanadium Alloy for Surgical Implant Applications, in: West Conshohocken, PA, 2014. doi:https://doi.org/10.1520/F1472-14
15. Henning M, Vehoff H (2007) Statistical size effects based on grain size and texture in thin sheets. Mater Sci Eng A 452–453:602–613. https://doi.org/10.1016/j.msea.2006.11.113
16. Carroll BE, Palmer TA, Beese AM (2015) Anisotropic tensile behavior of Ti-6Al-4V components fabricated with directed energy deposition additive manufacturing. Acta Mater 87:309–320. https://doi.org/10.1016/j.actamat.2014.12.054
17. Dzugan J, Seifi M, Prochazka R, Rund M, Podany P, Konopik P, Lewandowski JJ (2018) Effects of thickness and orientation on the small scale fracture behaviour of additively manufactured Ti-6Al-4V. Mater Charact 143:94–109. https://doi.org/10.1016/j.matchar.2018.04.003
18. Duffy M (2018) Microtensile characterization of additively manufactured Al-Si-10Mg, Ph.D. dissertation, University of Maryland Baltimore County